Accession No. 04430-65

SID 65-550

Copy No. 3

ENGINEERING METHOD TO PREDICT SATURN V VEHICLE AND LAUNCH COMPLEX ENVIRONMENTS DUE TO ROCKET JET IMPINGEMENT

QUARTERLY PROGRESS REPORT NO. 3
Contract NAS 8-11407

15 April 1965

Prepared by

A. Africano

A. Africano
Power and Environmental Systems

Approved by

F. G. Etheridge
Program Manager

W. H. T. Loh, Director
Power and Environmental Systems
Aerospace Sciences Division

NORTH AMERICAN AVIATION, INC.
SPACE and INFORMATION SYSTEMS DIVISION

FOREWORD

This is the third quarterly progress report submitted to the National Aeronautics and Space Administration, Marshall Space Flight Center, in partial fulfillment of the requirements on Contract NAS 8-11407. The report covers activity and progress achieved in the three-month report period 1 January through 31 March 1965. Acknowledgements of material contributed for the report by S&ID personnel other than the author are made as footnotes in the sections where used. The scope covered includes principally the Phase II Analytical and Experimental Correlation, with some remaining items, particularly on plume impingement geometry for curved surfaces, from the Phase I Analytical Investigations. The material in this report and in the preceding first and second quarterly progress reports will be compiled as a final report in the next quarterly period, with such changes as may be needed, to present the complete results of the 12-month investigation program on engineering methods to predict the force and heat loads due to rocket jet impingement on typical surfaces of space vehicles and launch structures.

This study program is under the direction of Mr. J. C. Cody, NASA/MSFC, Contracting Officer's Representative, and Mr. J. L. Moses, Alternate, of the George C. Marshall Space Flight Center, Propulsion and Vehicle Engineering Division, National Aeronautics and Space Administration, Huntsville, Alabama. Mr. F. G. Etheridge is the Program Manager for NAA/S&ID.

TECHNICAL REPORT INDEX/ABSTRACT

ACCESSION NUMBER	DOCUMENT SECURITY CLASSIFICATION
04430-65	Unclassified

TITLE OF DOCUMENT

Engineering Method to Predict Saturn V Vehicle and Launch Complex Evironments due to Rocket Jet Impingement, Quarterly Progress Report No. 3.

LIBRARY USE ONLY

AUTHOR(S)

A. Africano

CODE	ORIGINATING AGENCY AND OTHER SOURCES	DOCUMENT NUMBER
	NAA/S&ID Aerospace Sciences	SID 65-550

PUBLICATION DATE	CONTRACT NUMBER
15 April 1965	NAS 8-11407

DESCRIPTIVE TERMS

Rocket Jet Plume Environments
Exhaust Gas Impingement Effects
Impact Pressures
Heat Transfer due to Photon and Molecular Impact
Radiation, Conduction, and Convection Heat Transfer
Saturn V Vehicle
Prediction Methods

ABSTRACT

2 4/4 89

This report presents the results of investigations made during the third quarterly period of the study program under NASA/MSFC Contract NAS 8-11407. The material reported completes the Phase I Analytical Investigations and Phase II Analytical and Experimental portions of the 12-month program. The objective of the study is to correlate available experimental data on forces and heat loads induced by rocket jet plume impingement from sea level to near-vacuum environments with theoretical and empirical prediction methods. The configuration of the Saturn V Vehicle and Launch Complex environments is simulated by typical flat and curved surfaces.

Topics discussed in the report include:

1. A summary of the principal topics covered in previous quarterly progress reports Nos. 1 and 2.

2. Jet plume interaction with freestream, including influence coefficients for handling small changes in input variables.

3. Geometry of impingement on curved surfaces, including concave and convex cylinders parallel to the plume axis, canted cylinders, cylinders at right angles to the plume axis, and spheres.

4. Heat transfer due to jet impingement, with alternate prediction methods based on aerodynamic stagnation and turbulent flow analyses for correlating the Saturn SA-5 launch test data; an analysis of new concepts of the contributions of radiation, conduction and convection jointly making up usual experimental data, a proposed series of tests for isolating the separate effects, and analysis of the results by use of a new "characteristic velocity" of heat transfer coefficient of the basic impingement pressure.

author

TABLE OF CONTENTS

ILLUSTRATIONS

I. INTRODUCTION

This Third Quarterly Progress Report submitted by North American Aviation, Inc., Space and Information Systems Division (NAA/S&ID) to the National Aeronautics and Space Administration, George C. Marshall Space Flight Center (NASA/MSFC) on Contract NAS 8-11407, covers the contract performance period 1 January 1965 through 31 March 1965. The objective of the twelve-month program is to correlate theoretical or empirical prediction methods and the available experimental data on rocket jet plume impingement forces and heat loads. The structures affected by the plume impingement may be on the vehicle itself, on nearby vehicles, or on the launch tower and associated equipment, with the Saturn V Vehicle and Launch Complex utilized as a reference configuration, as illustrated in the first quarterly progress report, Reference (1). However, all cases of impingement effects are categorized and simplified for analysis within the scope of the effort as flat or curved surfaces at various distances aft of the rocket nozzle exit plane and radially displaced from the jet plume centerline.

The material in the present report completes the Phase I Analytical Investigations and the Phase II Analytical and Experimental Correlation portions of the planned program. Phase III comprises the generation of the Recommended Engineering Prediction Method which will be included in the forthcoming Final Report. As an aid in maintaining continuity of the present report with the two previous quarterly progress reports, following is a summary of the topics already reported upon:

Quarterly Progress Report No. 1 (SID 64-1896, dated 15 October 1965, Reference 1)

I. Introduction - Program Objectives

II. Basic Surface Environments of Space Vehicles and Launch Complex Structures

III. Jet Plume Free Flow Fields

IV. Interaction of Freestream with Jet Plume (basic theory).

V. Plume Impingement Geometry for Canted and Uncanted Side Plates

VI. Newtonian Impact Theory for Impingement on a Flat Plate

VII. Convective Heat Transfer due to Jet Impingement (oblique shock region)

VIII. Plume Radiation Study (molecular radiators)

Quarterly Progress Report No. 2 (SID 65-44, dated 15 January 1965, Reference 2)

I. Introduction

II. Jet Plume Free Flow Field with Varying Specific Heat Ratio

III. Jet Plume Interaction with Free Stream (preliminary plume contraction results)

IV. Approximation of Sea Level Jet Plume Properties

V. Impingement Pressure Correlation (for sea level SA-5 launch data and Apollo Reaction Control Engine high-altitude chamber data)

VI. Convective Heat Transfer Correlation (results for oblique shock region, and prediction equation for normal shock region)

VII. Plume Radiation Study (solid-particle radiation)

The results of the investigations during the first six months study showed that the prediction methods compiled or developed gave good correlation with experimental data for both the impact pressures and heat transfer rates for the high-altitude plumes; and for the impact pressures only for the low altitude, or sea level plumes. The experimental impingement pressures for the Saturn SA-5 launch were closely matched by the predictions; however, additional investigations of applicable aerodynamic heating analyses were found necessary to match the very high test heating rates, in this case. Results of the alternate heat transfer prediction methods were successful in correlating the test data within the apparent experimental error, and are included in the present report, together with a discussion of basic concepts on the relation of heat transfer and impingement pressure and proposed test setups for future continued study and experimentation.

In addition, this report includes the remaining Phase I analytical investigations of the impingement geometry for concave and convex cylinders parallel to the plume axis; for a canted cylinder; for a convex

cylinder at right angles to the plume axis; and for a sphere (representing the leading surface of a blunt immersed body most frequently treated in the related aerodynamic satellite reentry heating studies.) In each case, the desired result is the sine function of the true streamline impingement angle which appears in the impact pressure prediction equation.

II. JET PLUME INTERACTION WITH FREESTREAM

The basic equations for use with the method of characteristics were presented in the first quarterly progress report. Initial results of the combined computer program (AP-214 "Freestream") were given in the second progress report showing how the width of the plume from a moving rocket was contracted from its free flow field width as a function of the freestream Mach number, M_∞, for a series of planes located 1, 2, 5, 10, and 15 nozzle exit radii downstream of the exit plane. The case selected for study was for a nozzle exit Mach number $M_e = 3.0$, exit specific heat ratio $k = 1.3$ (assumed constant during subsequent plume expansion), ratio of total pressure at exit to ambient pressure $p_T/p_\infty = 10{,}000$, and nozzle exit half-cone angle $\theta_N = 15°$. The effect of varying the specific heat ratio during plume expansion was discussed and results presented for the case of the free flow field plume of a non-moving nozzle. In order to determine the effects with the freestream interaction for the moving nozzle, the following variables were considered in the past report period:

1. Specific heat ratio of 1.2, instead of 1.3, to provide a large percent change in the event that the effect was small (as proved to be the case),

2. Nozzle half-cone exit angle of 10° instead of 15° to provide a closer approximation to the more typical design condition of the larger area expansion ratio nozzle,

3. Exit total to ambient pressure ratio of 100, instead of 10,000, to provide conditions simulating a lower altitude nozzle design.

All of these cases were computed using the same nozzle exit Mach number of 3.0 as a reference value, constant specific heat ratio of 1.4 for the freestream (air), and freestream Mach numbers of 0, 5, and 10, except in one case with the combined lower pressure ratio and exit angle, for which a solution was obtained only for $M_\infty = 0$ and 2.

The results showing the effects of the two specific heat ratios and exit angles on the contraction of the plume boundary are shown in Figures 1 and 2. As anticipated, the effects of the range of specific heat ratio and nozzle angle excursion tested had only relatively small influence on the contraction ratio for all freestream Mach numbers, particularly after the first few exit radii downstream of the nozzle exit. For example, from Figure 1, the plume contraction ratios at the dimensionless downstream distance $x/R_e = 5$, for freestream Mach numbers

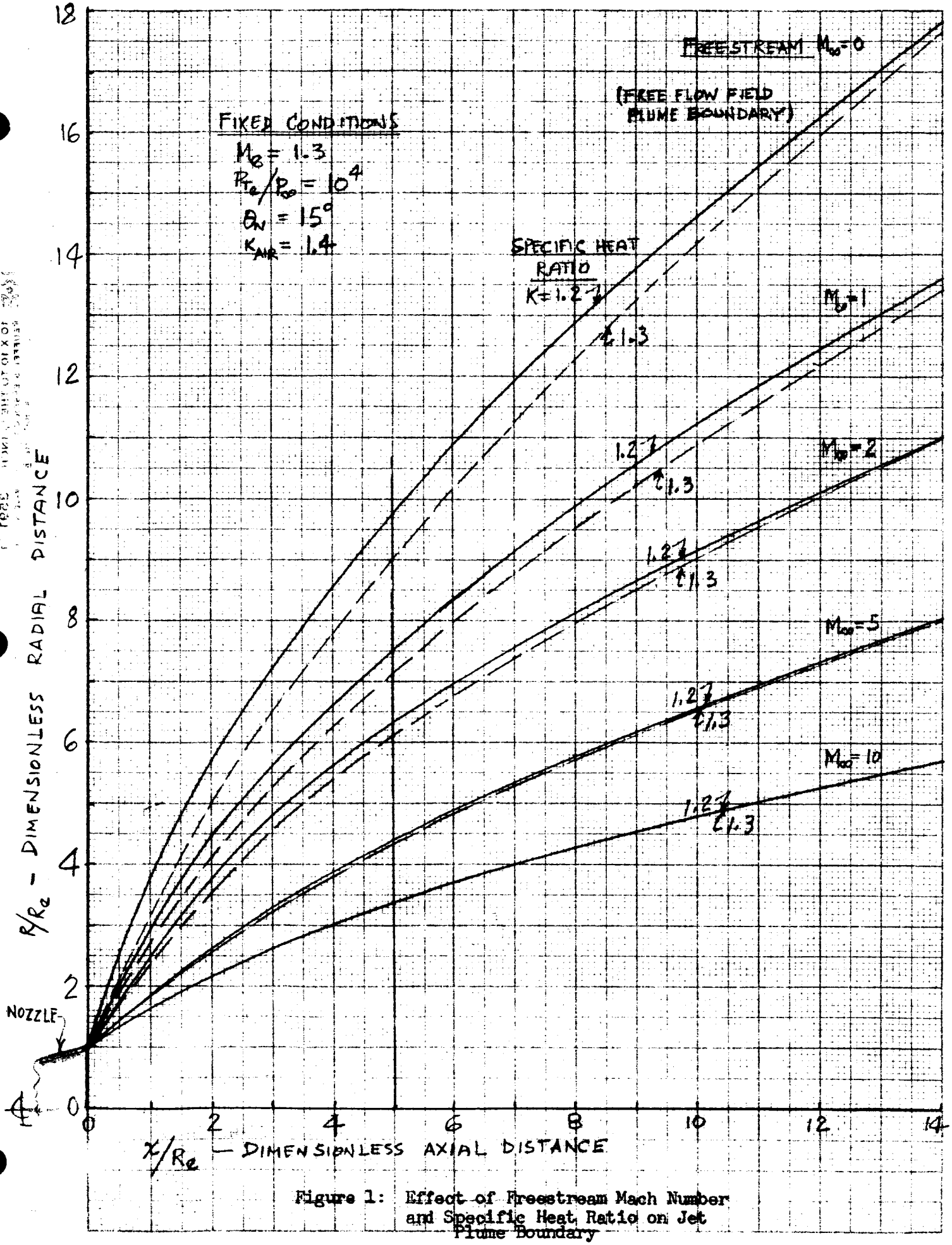

Figure 1: Effect of Freestream Mach Number and Specific Heat Ratio on Jet Plume Boundary

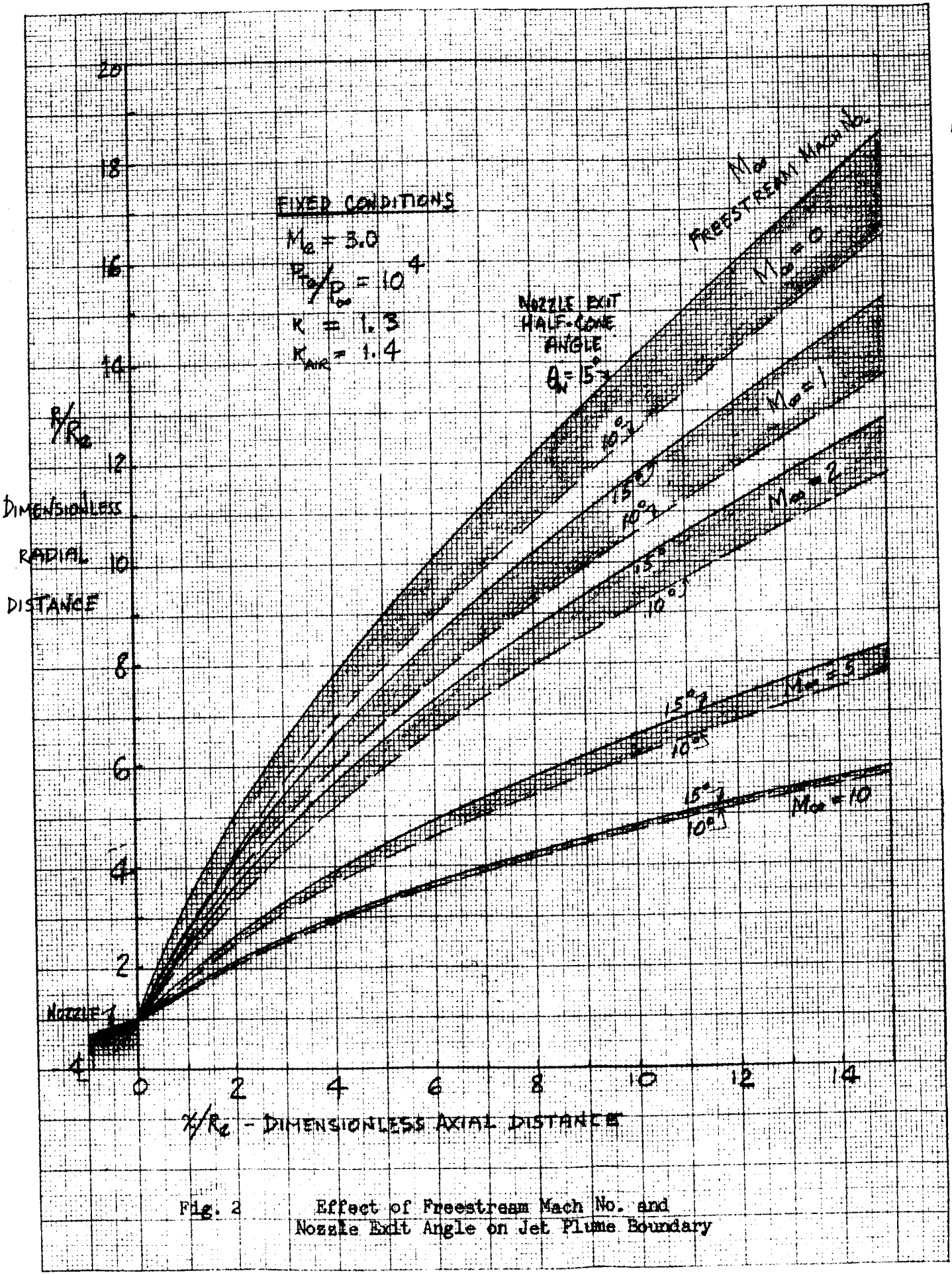

Fig. 2 Effect of Freestream Mach No. and Nozzle Exit Angle on Jet Plume Boundary

of 0, 1, and 2, using the specific heat ratio k = 1.3 as the reference, are 9.1/9.1, 7.0/9.1, and 6.0/9.1, or 1.00, 0.77, and 0.66, respectively. The ratios corresponding to a change in k of (1.2-1.3/1.3) 100 = -7.7% are then 9.8/9.1, 7.3/9.1, and 6.2/9.1, or 1.08, 0.80, and 0.68, respectively.

Dividing the percent changes in the ratios, by the percent change in the varied parameter now indicates that the contraction ratios for M_∞ = 0, 1 and 2 are 1.04, 0.39, and 0.26% higher than the reference values due to 1% decrease in the specific heat ratio.

Similarly, from Figure 2, the contraction ratios for M_∞ = 0, 1, and 2 at x/R_e = 5 may be calculated as 0.33, 0.30, and 0.23% lower than the reference values due to 1% decrease in the nozzle half-cone exit angle. Of course the reference nozzle half-cone angle could be selected preferably at 10°, as a more representative case, and the resulting percent contraction changes for M_∞ = 0, 1, and 2, then would be + 0.38, + 0.34, and + 0.23, respectively, at the same x/R_e distance, for a + 1% increase in θ_N .

Similar influence coefficients for the principal variables entering into the jet plume calculation could be determined over a variety of plume environments. The preliminary results indicate that the concept of a broad band of practical sea level and in-flight jet plume descriptions handled by a judicious choice of such influence coefficients may be feasible, due to the small effects of many of the variables. Since the very large number of possible combinations of the variables precludes making general tables of plume descriptions covering all cases, an approach to this goal in future investigations would be the determination of sets of influence coefficients applicable to selected "standard" plumes for low, intermediate, and high altitude environments.

III. GEOMETRY OF IMPINGEMENT ON CURVED SURFACES

The simplest case of jet plume impingement on a flat plate or plane parallel to the axis of the axisymmetric plume was analyzed together with the next simplest case of a canted plate in the first quarterly progress report (Reference 1). Since an elemental area on any curved surface fits into the category of a canted plane, the obvious practical expedient frequently used for solution of impingement pressures on complex shapes has been to divide up the complex surface into a series of canted planes, locate these with respect to the nozzle exit reference origin, and then proceed with this approximate type of solution.

However, except for typical structural members of the launch umbilical towers and pads, most actual cases of impingement surfaces are more accurately described as portions of the concave and convex surfaces of cylinders whose longitudinal axes are parallel, axially canted, or at right angles to the plume axis, or as a portion of the convex surface of a sphere. Explicit solutions for these typical cases are desirable. Original derivations based on the consistent use of standardized jet plume flow field parameters in the analytical solid geometry are presented in the following sections. These include the cases of impingement on the surfaces of:

(a) The concave cylinder parallel to the plume axis,
(b) The convex cylinder parallel to the plume axis,
(c) The convex cylinder canted to the plume axis,
(d) The convex cylinder at right angles to the plume axis, and
(e) The sphere.

While the most complex case might have been derived first and the results then reduced to those for the simpler cases, the development proceeding from the simpler cases serves to emphasize the visualization technique leading to the generally similar methods of solution. For simplicity and better understanding of the geometrical analysis, the actual plume distances x_p from the nozzle exit plane and the radial distances R from the plume axis are depicted in the diagrams and used in the derivations rather than the customary dimensionless distances x_p/R_e and R/R_e relative to nozzle exit radius, R_e. However, the resulting equations are applicable using these dimensionless plume parameters provided all other dimensions including those describing the surfaces are read as dimensionless ratios relative to R_e.

A. Concave Cylinder Parallel to Plume Axis

The geometry of impingement was analyzed for the case of the canted plate in the first quarterly progress report to determine the

true impingement angle, θ_I, in terms of the known jet plume description parameters, x, R, and θ, for use in the impact pressure equation

$$p_I = \rho V^2 \sin^2 \theta_I \qquad (1)$$

The sine of the true impingement angle is similarly required for the cases of impingement on curved surfaces. As illustrated in Figure (3a), the plane tangent to the curved surface at the point of impingement, P, must now be considered in place of the canted plate, to determine the true angle APE, or θ_I . Since the axis of the cylinder in the XX direction is parallel to the plume axis, the view in the XZ plane shows the true length of the perpendicular BD dropped from the axis end "A" of the streamline tangent AP to the tangent plane DP (shown as AE in the perspective view on the left.) These lengths can be evaluated using plane analytical geometry as follows:

BD is the cosine projection of the radial distance R of impingement point P from the axis. The angle DBP, or α, is the same as the alternate interior angle BPC between parallel lines BD and PC, and evaluated by the cosine relation for the plane oblique triangle BPC with three sides known. The length AP is simply defined in terms of the plume parameters, as R/sin θ. Dividing, and simplifying these results leads to the desired value of sin θ_I in terms of the known cylinder radius, R_c, and location of the cylinder axis in the YZ plane, Z_c, and the known jet plume parameters, R, and the angle θ made by the tangent to the streamline at point P and the plume axis:

$$\sin \theta_{I_{cc(x)}} = \frac{R_c^2 + R^2 - Z_c^2) \sin \theta}{2 R_c R} \qquad (2)$$

for the case of impingement on the concave surface of a cylinder whose axis is parallel to the plume axis.

Solutions would be made for a series of radial distances, R_o, R_1, R_2, etc., from the plume axis, with impingement occurring from the minimum value, $R_o = R_c - Z_c$, to the maximum aalue, $R_c + Z_c$, and repeated for as many transverse planes located at distances x_1, x_2, etc., as needed, to envelop the particular cylindrical shape subjected to impingement.

The locations of the impingement points on the cylinder in each X-plane are obtained from simultaneous solution of the equations of the plume impingement circle with radius R and the cylinder circle with radius R_c, or from:

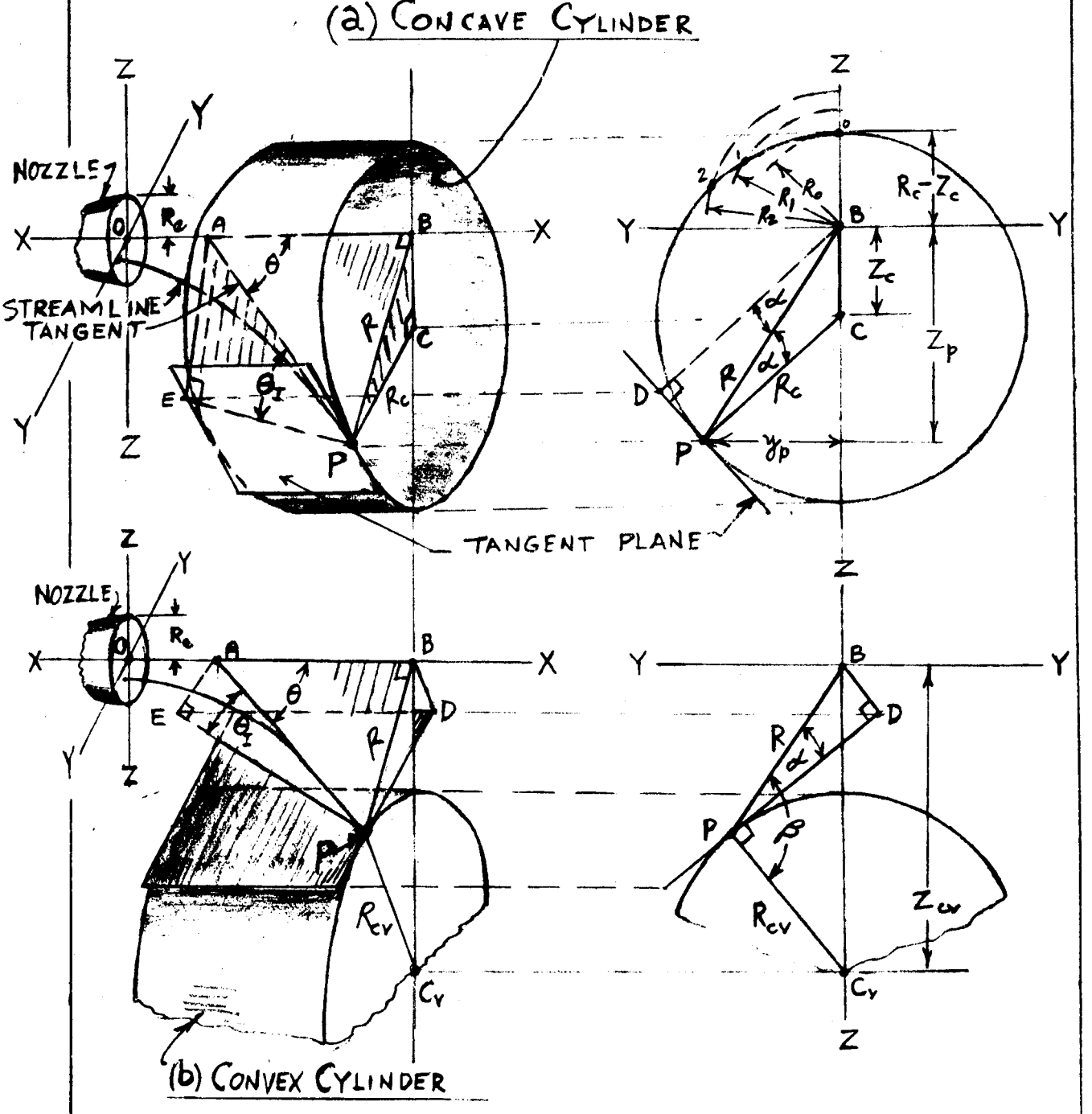

Fig. 3 Geometry of Impingement of Plume Streamline on Concave and Convex Cylinders Parallel to Plume

$$R^2 = Z_p^2 + y_p^2 \tag{3}$$

$$R_c^2 = (Z_p - Z_c)^2 + y_p^2 \tag{4}$$

which yield $$z_p = \frac{Z_c^2 + R^2 - R_c^2}{2 Z_c} \tag{5}$$

and $$y_p = \sqrt{R^2 - Z_p^2} \tag{6}$$

In the case of a cluster of nozzles, a first approximation to the total impingement pressures would be obtained by using the principle of superposition, or simple summation of the individual plume pressure contributions. This may be sufficient to indicate maximum pressure locations. A second approximation could include the effects of primary mutual impingement of the plumes on phantom separation walls, and then the secondary impingement of the resulting composite plume on the actual wall surface. Such estimates are needed also to establish the aft and forward (reverse) flows for base pressure and heating investigations. These calculations are complex and should be made for specific applications where the detailed geometry and engine plume descriptions are available, but are outside the scope of the present effort to establish the basic engineering techniques.

B. Convex Cylinder Parallel to Plume Axis

Figure (3b) shows the elements of this case. Again the true value of sin θ_I is desired. The required right triangle consisting of the perpendicular to the tangent plane and the tangent to the streamline is shown as AEP in the perspective view, and as BDP in the YZ plane view. The true length of the perpendicular is BD in the latter view, and the true length of the tangent AP, in terms of the plume flow field parameters, is $R/\sin\theta$. Thus, sin θ_I = BD(or AE)/AP, or $R \sin\alpha / (R/\sin\theta) = \sin\alpha \sin\theta$.

The angle BDP, or α, is evaluated by observing that $\beta = 90° + \alpha$, and $\sin\alpha = \cos\beta$. Using the cosine law of plane geometry to solve for cos β in triangle BPC_v, with side PB = R, side $BC_v = Z_{cv}$, and side $PC_v = R_{cv}$, we have

$$\cos\beta = \frac{R_{cv}^2 + R^2 - Z_{cv}^2}{2 R_{cv} R} \tag{7}$$

The desired sine function of the true impingement angle then becomes

$$\sin \theta_{I_{cv}} = \frac{(Z_{cv}^2 - R_{cv}^2 - R^2) \sin \delta}{2 R_{cv} R} \qquad (8)$$

for the parallel convex cylinder surface impingement.

As before, a series of solutions are required in each transverse section, and sufficient transverse sections considered to envelop the portion of the cylinder under impingement. The same equations apply for locating the impingement points as given above for the case of the concave cylinder (Equations 3 to 6).

C. Canted Convex Cylinder

This case, illustrated in Figure (4) is typical for the impingement of angled pitch and yaw, reaction control engine plumes on the vehicle cylinder. The location of the cylinder axis relative to the plume coordinate system is defined by the cant angle δ and the perpendicular distance "a" from the nozzle exit center origin to the nearest element of the cylinder. The elliptical section of the cylinder cut by a transverse plume plane at distance x_p from the nozzle exit is shown in View A-A, and a transverse plane through the cylinder cutting the plume axis at its intersection with the streamline tangent AP is shown as Section B-B. The location of the coordinates of the streamline impingement point on the cylinder is determined by simultaneous solution of the equation of the circle of plume radial distance R (with x_p constant):

$$R^2 = y_p^2 + Z_p^2 \qquad (9)$$

and the equation of the elliptical section of the cylinder in View A-A:

$$\frac{(Z_p - Z_c)^2}{(R_c/\cos \delta)^2} + \frac{y_p^2}{R_c^2} = 1 \qquad (10)$$

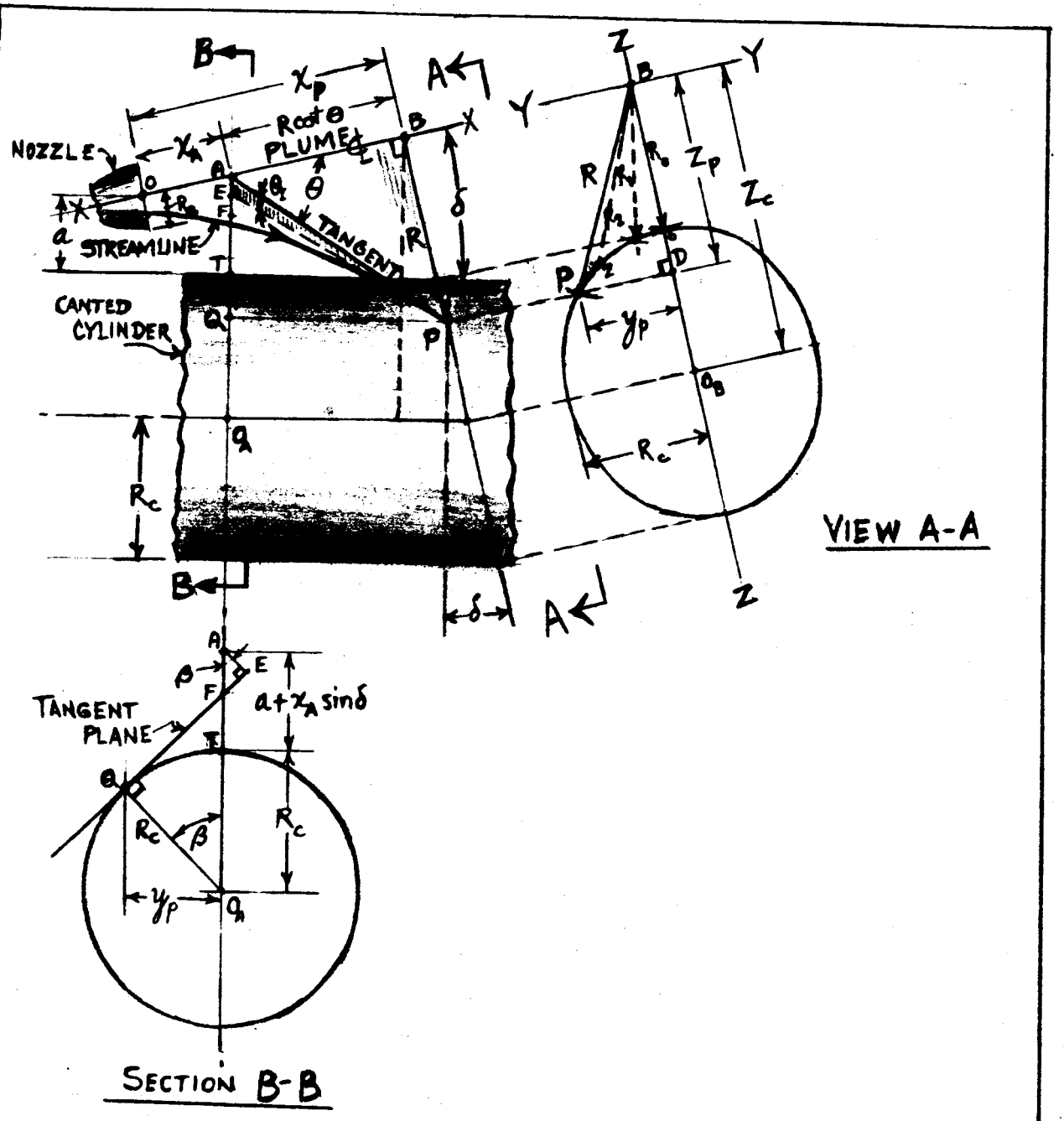

Fig. 4 Geometry of Impingement of Plume Streamline on Canted Convex Cylinder

which yields

$$Z_p = \sqrt{Z_c^2 \cot^4\delta + (R^2 - R_c^2 + Z_c^2 \cos^2\delta)/\sin^2\delta} - Z_c \cot^2\delta \quad (11)$$

For small angles, substitution of $\cos \delta \doteq 1$, and $\sin \delta \doteq \delta$ in Eq. (11) results in the same value for Z_p as Eq (5) for the case of the parallel cylinder. As before, y_p is then evaluated from Eq (9) as $\sqrt{R^2 - Z_p^2}$. Since Z_c varies for each selected value of x_p, it must be evaluated to complete the solution of the above equations. From the given geometry

$$Z_c = (a + x_p \sin \delta + R_c)/\cos \delta \quad (12)$$

Section B-B in Figure (4) provides the plane geometry for calculating the required perpendicular distance AE to the tangent plane EFQP from the similar right triangles O_AQF and FEA. Thus

$$AE = AF \cos \beta = (AO_A - FO_A) \cos \beta$$

$$= (a + x_A \sin \delta + R_c - R_c/\cos \beta)\cos\beta$$

with $$\cos \beta = \sqrt{1 - \sin^2\beta} = \sqrt{1 - (y/pR_c)^2}$$

and the tangent length $AP = R/\sin \theta$, the desired since function of the true impingement angle θ_I becomes

$$\sin \theta_{I_{ccv}} = \sin \theta\left[(a + x_a \sin\delta + R_c)\sqrt{1 - (y_p R_c)^2} - R_c\right]/R \quad (13)$$

When the cant angle approaches zero, Eq. (13) reduces to Eq. (8) for the case of the parallel convex cylinder.

D. Convex Cylinder at Right Angles to Plume Axis

This case is typical for reaction control roll engines having their thrust directed at right angles to the vehicle cylinder axis. Figure (5) shows a transverse section of the cylinder in a longitudinal section of the rocket plume. The locations x_c, and y_c of the center of the cylinder relative to the reference nozzle exit origin, O, are needed together with a series of streamline tangent angles θ_o, θ_1, θ_2, and radii from the plume axis, R_o, R_1, R_2, for each transverse plane of the plume at distance x_p. A single tangent plane CDP_oP illustrated in the perspective sketch "A" serves to locate all points of intersection

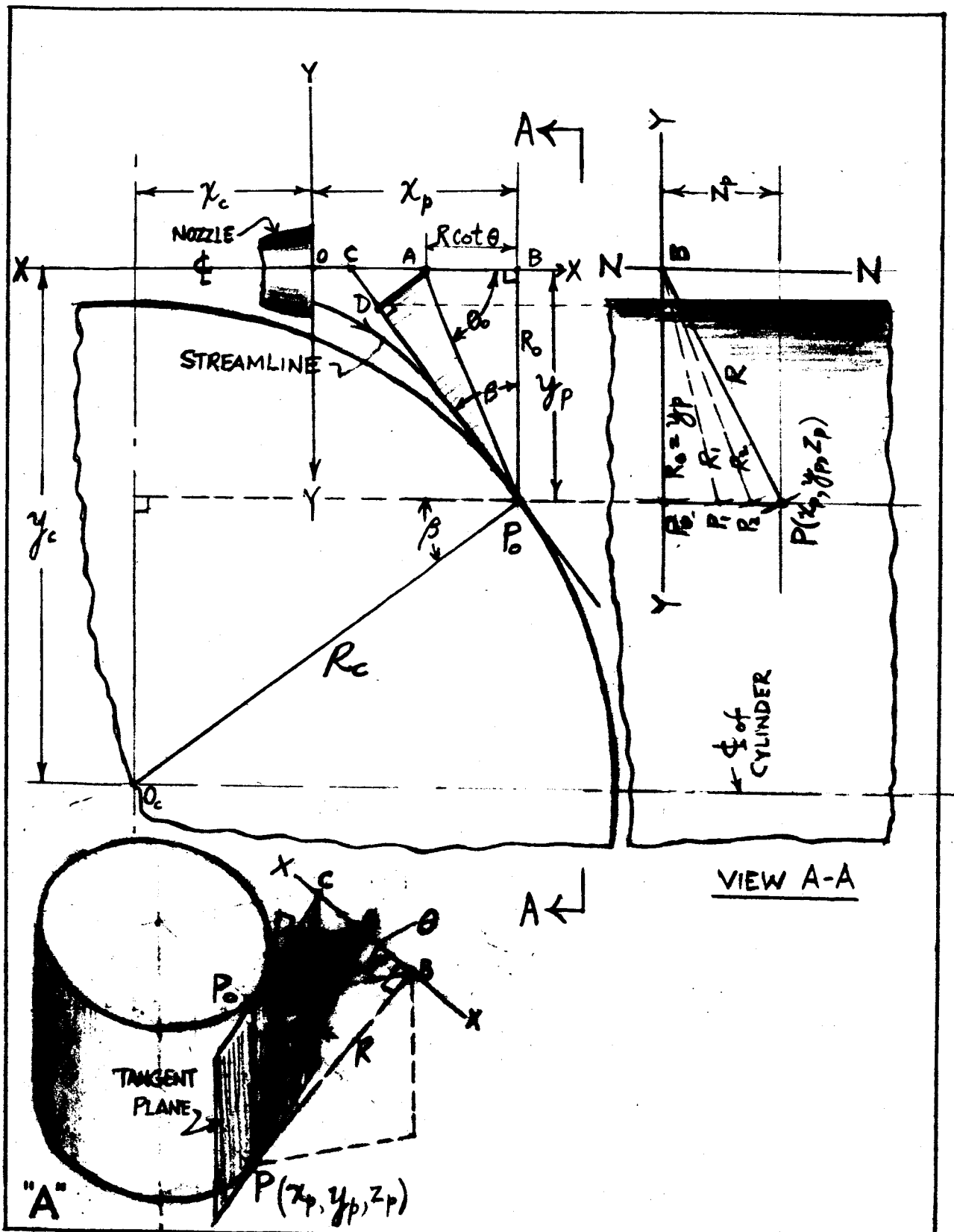

Fig. 5 Geometry of Impingement of Plume Streamline on Convex Cylinder at Right Angles to Plume Axis

of the impinging streamlines for each x_p plume plane. The true impingement angle θ_I is APD in this sketch, and the desired sine function can be evaluated as AD/AP, where AP is the tangent to the streamline and known from the plume flow field description parameters as R/sin θ. The perpendicular distance of the plume axis end of this tangent line to the tangent plane is always AD which is found from the right triangle ADP_o .

The location of the impingement point on the cylinder surface is determined from the simultaneous solution of two equations of circles:

$$R^2 = y_p^2 + Z_p^2 \tag{14}$$

for the plume radial distance circle, and

$$R_c^2 = (x_p - x_c)^2 + (y_p - y_c)^2 \tag{15}$$

for the cylinder.

Thus, since x_p is assumed constant for each plume section considered, Eqs. (14) and (15) now provide the remaining coordinates of the impingement point $P(x_p, y_p, Z_p)$.

The angle AP_oD is $(\beta - \theta_o)$ where β is $\sin^{-1} (y_p - y_c)/R_c$ and θ_o is $\tan^{-1} y_p$ (or R_o)/R cot θ. Then

$$AD = AP_o \sin (\beta - \theta_o)$$
$$= \sqrt{R^2 \cot \theta^2 + y_p^2} \sin (\beta - \theta_o)$$

and the sine of the true impingement angle θ_I is:

$$\sin \theta_{I_{rc}} = \frac{\sqrt{R^2 \cot \theta + y_p^2} \sin (\beta - \theta_o)}{R/\sin \theta} \tag{16}$$

When $R = R_o = y_p$, and $\theta = \theta_o$, the angle AP_oD or $\beta - \theta_o$ in the plane of the page of Figure (5) becomes the true impingement angle, and for this special case of the minimum radial distance $R = R_o$, Eq (16) reduces to

$$\sin \theta_{I_o} = \sin (\beta - \theta_o) \tag{16a}$$

E. Sphere

Figure (6) shows the elements of the impingement problem for spherical surfaces partly or wholly immersed in the plume flow field. The familiar special case of a hemispherical blunt leading edge in aerodynamic flow would be obtained when the spherical center location $Z_s = y_s = 0$. As in all preceding cases the result sought is the sine function of the true impingement angle θ_I in the plane perpendicular to the tangent surface at the point of impingement. Again, a series of transverse planes transverse to the plume axis must be considered to obtain the full range of impingement. The YZ planes intersect the sphere in circles whose radii can be determined, together with the remaining coordinates y_p and Z_p of the impingement point in terms of the known plume and sphere parameters, by simultaneous solution of the following three equations:

(1) As before, the equation of the circle for the radial distance R of the impingement point from the plume axis:

$$R^2 = y_p^2 + Z_p^2 \tag{17}$$

(2) The equation of the circle of intersection with the sphere in the x_p plane:

$$r_p^2 = (y_p - y_s)^2 + (Z_p - Z_s)^2 \tag{18}$$

(3) The equation of the sphere:

$$R_s^2 = (x_p - x_s)^2 + (y_p - y_s)^2 + (Z_p - Z_s)^2 \tag{19}$$

The insert sketch "A" in Figure (6) indicates that the minimum plume radial distance R_o to be considered is:

$$R_o = \sqrt{y_s^2 + Z_s^2} - R_s \tag{20}$$

and the maximum plume radial distance,

$$R_{max} = \sqrt{y_s^2 + Z_s^2} \tag{21}$$

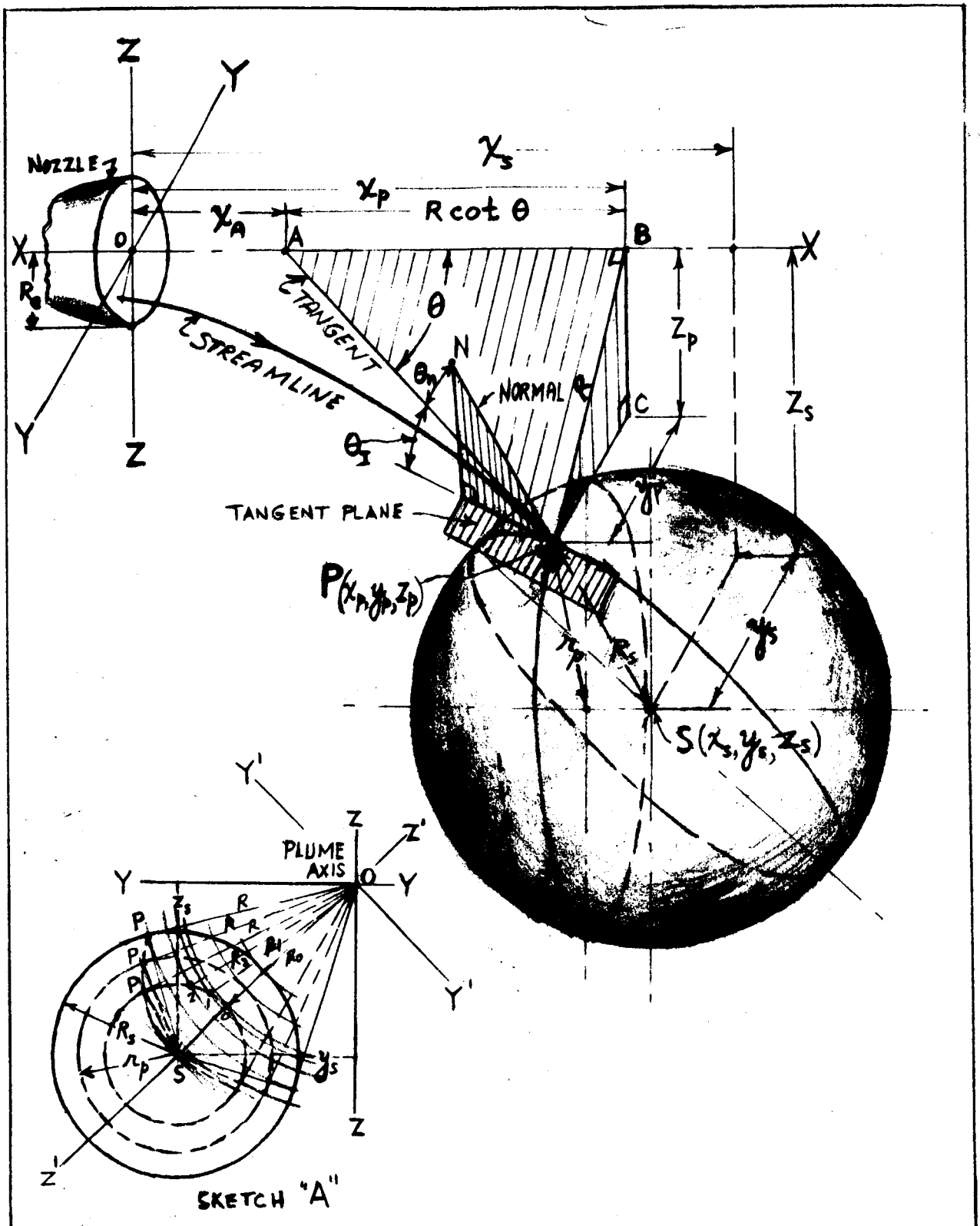

Fig. 6 Geometry of Impingement of Plume Streamline on Sphere

It is convenient in this case to determine the cosine of the complementary angle θ_n between the normal to the sphere at the point of impingement P and the streamline tangent AP as equivalent to the desired sine of the true impingement angle θ_I, or

$$\sin \theta_I = \cos \theta_n \tag{22}$$

with x_A equal to $x_p - R \cot \theta$, and $y_A = Z_A = 0$ on the plume axis, the axis end coordinates of the space tangent line AP are known. After the impingement point coordinates are evaluated from Equations (17), (18), and (19), the direction cosines of this tangent can be determined. The coordinates of two points, P and S on the normal NPS are now also known, so that its direction cosines likewise can be determined.

The cosine of the angle formed by the intersecting tangent AP and normal PS in terms of the two sets of direction cosines now may be found from the relation given in solid analytical geometry textbooks (e.g., see Reference (3)):

$$\cos \theta_n = \cos \alpha_t \cos \alpha_n + \cos \beta_t \cos \beta_n + \cos \gamma_t \cos \gamma_n \tag{23}$$

where the subscripts, t and n, refer to the tangent and normal lines, and the space angles α, β, and γ are the angles formed between the lines and the X, Y, and Z coordinate axes, respectively.

The direction cosines are defined by the ratios of the line intercepts parallel to XY, ZY, and ZX planes to the lengths of the lines between their two known point locations. Then, since the tangent length is known in terms of the plume parameters as $R/\sin \theta$, and the portion of the normal length PS is the given spherical radius, R_s, the direction cosines may be written as:

$$\cos \alpha_t = (x_p - x_Z)/(R/\sin \theta) \tag{24}$$

$$\cos \beta_t = (y_p/(R/\sin \theta) \tag{25}$$

$$\cos \gamma_t = Z_p/(R/\sin \theta) \tag{26}$$

for the tangent line, and as

$$\cos \alpha_n = (x_p - x_s)/R_s \tag{27}$$

$$\cos \beta_n = (y_p - y_s)/R_s \tag{28}$$

$$\cos \gamma_n = (Z_p - Z_s)/R_s \tag{29}$$

for the normal line.

Substituting the values of the direction cosines from Equations (24) to (29) into Equations (23) and (22) yields the desired sine function of the true impingement angle as

$$\sin \theta_{I_S} = \frac{\sin \theta}{R_s R}\left[x_p - x_A)(x_p - x_s) + y_p\,(y_p - y_s) + Z_p(Z_p - Z_s)\right] \quad (30)$$

Note: As stated at the beginning of Section IV, all dimensions indicated by x_p, x_A, x_s, y_p, y_s, Z_p, Z_s, R_s and R in Eq. (30), and similar dimensions in the final equations for the preceding cases, can be considered to be divided by the radius R_e of the nozzle in the exit plane, thus made dimensionless and compatible with the customary dimensionless plume parameters, x/R_e and R/R_e.

IV. HEAT TRANSFER DUE TO JET IMPINGEMENT

A. Correlation of SA-5 Thermal Data

Computed results were presented in the previous quarterly progress report demonstrating that the predicted heat transfer rates due to jet plume impingement on a canted side plate were in satisfactory correlation with the experimental results obtained in a high altitude test chamber ($\approx$ 250,000 ft). The variables checked included: nozzle area expansion ratio, impingement plate side distance from the nozzle and its cant angle, plume and impingement distance downstream of the nozzle exit plane, lateral displacement distance from the centerline of the impinged plate and plate temperature. However, when Eq. (9), p. 28 of Reference (2), was applied to the sea level test data from the SA-5 launch, the predicted value of 224 BTU/ft^2 sec fell far short of the reported maximum measured value of about 1100 BTU/ft^2 sec for Data Point No. 2.

Since Eq. (9) was adapted from the empirical results of prior hypersonic aerodynamic reentry heating investigations for satellites (velocity, 20,000 ft/sec and above) and also to fit the different geometry of the Apollo RCS engine "freestream" flow and the canted side plate in the Tullahoma test set-up, it is not surprising that the major change in the environmental conditions to those of a booster engine at sea level strained the applicable empirical range. The results of the plume radiation study indicated only an almost negligible additional 22 BTU/ft^2 sec radiating from the 40-ft length of viewed plume (before impingement) for this case. The approximate geometry of the plume impingement on the instrumented hold-down unit is shown in Figure (7) for the two data points selected for this correlation study.

During the technical discussions and contract status review held at Huntsville on 27-28 January 1965 with Messrs. J. Cody and K. Mitchell, it was suggested that the local flow field after a normal shock impingement be investigated. It was thought that the high shock and/or stagnation temperatures existing very near the instrumented plate surfaces could contribute a substantial portion of the difference between the predicted convective heat transfer rate and the high measured rate. This calculation was made, but even with favorable assumptions such as full emissivity, configuration factor, and stagnation temperature recovery, the maximum thermal radiation rate was indicated to be only about 18% of the experimental 1100 BTU/ft^2 sec. It is of interest to note that a similar discrepancy between predicted and experimental heat transfer was reported by Cose and Fee in a recent Technical Note in the AIAA Journal (Reference 4). They found that for a solid propellant rocket plume impinging on a nearby side plate, "heat transfer in the impingement zone was 500 to 600% higher than a turbulent boundary-layer analysis would predict, (and) in this region, radiation was approximately

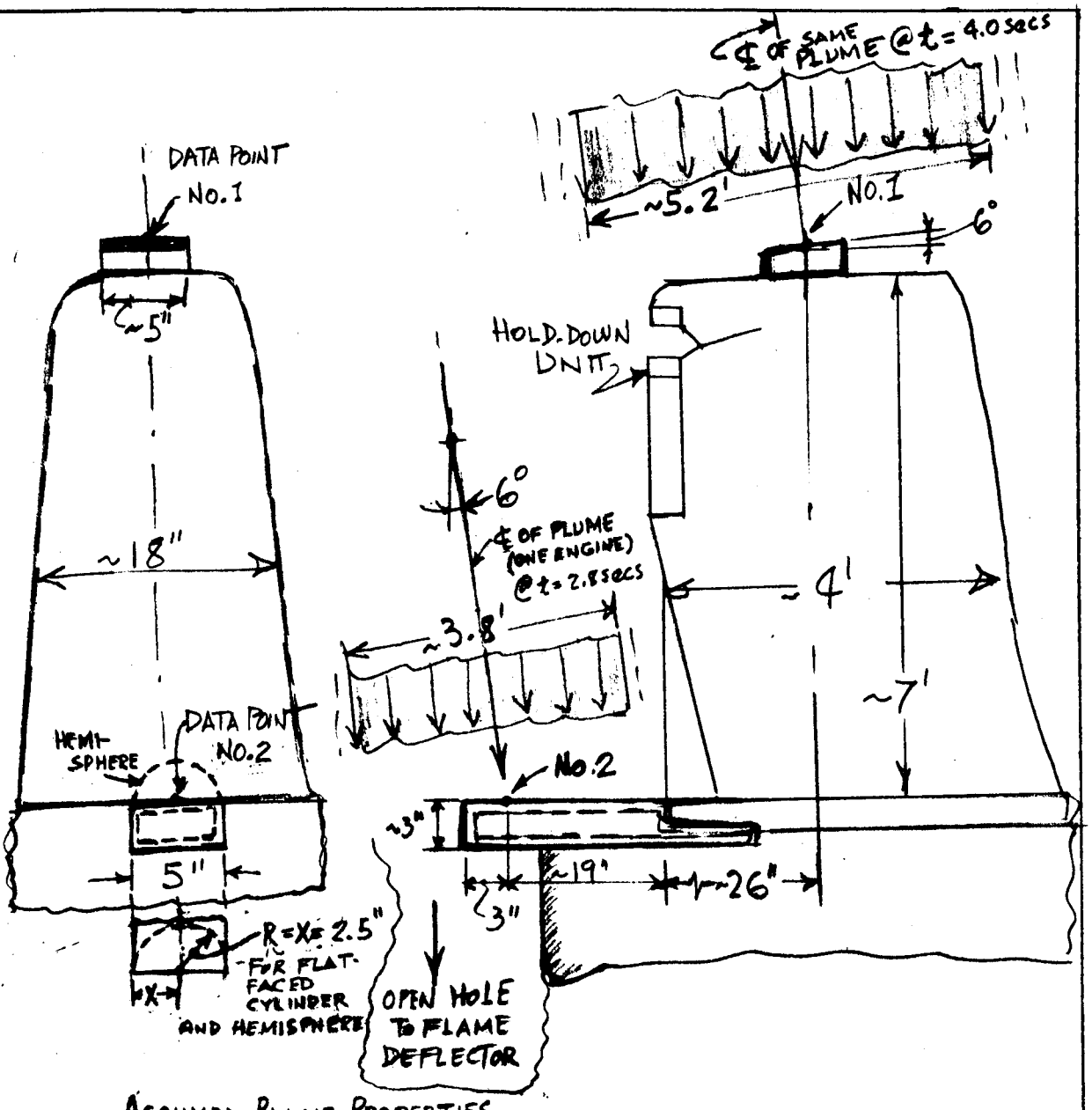

ASSUMED PLUME PROPERTIES BEFORE IMPINGEMENT

	DATA POINT NO. 1	DATA POINT NO. 2
Velocity, f/s	3200	5900
Density, slugs/ft³	3.8×10^{-4}	3.4×10^{-4}
Temp., °R.	2700	2900
Gas Constant	61	67
Pressure, psia	14.7	14.7
Spec. Heat Ratio	1.23	1.23

Figure 7. Approximate Geometry of Plume and Instrumented Data Points Nos 1 and 2 for SA-5 Launch Data Correlation

20% of the total heat transfer."

In the case under consideration (Data Point No. 2), the full stagnation temperature, T_s, (with estimated upstream plume static temperature and velocity before impingement $T_1 = 2900°R$, and $V_1 = 5900$ ft/sec, respectively, gas specific heat ratio and gas constant, $k = 1.23$ and $R_g = 67$ ft lb/lb °R respectively), is

$$T_s = T_1 + V_1^2 / (2gkR_g)/(k-1) \qquad (31)$$

$$= 2900 + 5900^2 / \left[(64.4 \times 1.23 \times 67)/(.23)\right]$$

$$= 2900 + 1510 = 4410 \ °R$$

The maximum theoretical prediction for the thermal radiation from a flat shock disc at this temperature, which is so close to the instrumented plate that a configuration factor of one may be assumed, is:

$$q_{rs} = \sigma \epsilon F (T_s^4 - T_w^4) \qquad (32)$$

where q_{rs} = stagnation value of thermal radiation, BTU/ft^2 sec

σ = Stefan-Boltzmann constant

$= 0.475 \times 10^{-12}$ BTU/ft^2 sec (°R)^4,

ϵ = net emissivity (assumed = 1)

F = configuration factor (assumed = 1)

T_s = stagnation temperature, °R, and

T_w = wall temperature °R (effect of $(T_w)^4$ assumed negligible)

Inserting the estimated and assumed values of the parameters in Eq. (32) yields

$$q_{rs} = 180 \text{ BTU/ft}^2 \text{ sec.}$$

Assuming the radiation from the non-impinging, but viewed, plume to be additive, the maximum predictable radiation heat transfer for Data Point No. 2 becomes 22 + 180 = 202, or as stated earlier, about 18% of the average of the two maximum measurements 1000 and 1200 BTU/ft^2 sec. This result indicates that the quoted estimate of about 20% of the total heat transfer attributed in Reference (3) due to radiation is about right. Even if it were as high as the 30% estimated by NASA/MSFC calculations, the remaining discrepancy would still be great enough to require consideration of alternate convective heat transfer relationships for the low altitude plume impingement environments. Two such alternates are described in the following section.

B. Alternate Convective Heat Transfer Relations

1. Stagnation Surface Heating Analysis*

Hoshizaki's simplified equation for stagnation surface heating (Reference (5) may be expressed as:

$$q_s = 2.59\sqrt{\frac{P_s}{V_{vac}}}\sqrt{\frac{dV}{dx_s}}\left[\frac{V_{vac}}{10{,}000}\right]^{2.19}\left(1 - \frac{h_w}{h_s}\right) \qquad (33)$$

where q_s = stagnation surface heat transfer rate, BTU/ft^2 sec,

P_s = stagnation surface pressure, psfa, evaluated from the upstream static pressure, p_1 = 14.7 psia; mass density,

$\rho_1 = 3.4 \times 10^{-4}$ slugs/ft^3; and plume velocity,

V_1 = 5900 ft/sec, for Data Point No. 2 as $\rho_1 V_1^2 + p_1 =$

$3.4 \times 10^{-4} (5900)^2 + 14.7 \times 144$

$= 11840 + 2120$

$= \underline{13950}$ psfa,

V_{vac} = vacuum gas velocity corresponding to total gas enthalpy, h_s, at upstream conditions,

$= V_1\sqrt{T_s(T_s - T_1)} = \sqrt{2gJ}\sqrt{h_s}$

$= 5900\sqrt{4410/(4410-2900)} = 224\sqrt{2040}$

$= 10{,}100$ ft/sec; making $P_s/V_{vac} = 1.175$, and

$\left[V_{vac}/10{,}000\right]^{2.19} = 1.02$,

$\left(\frac{dV}{dx}\right)_s$ = the stagnation point velocity gradient (sec^{-1}).

*The material presented in this section on stagnation surface heating, and in the next on turbulent flat plate heating, is based on the results of a study made for Power & Environmental Systems by G. M. Hanley and R. Norcross, of the NAA/S&ID Aerospace Sciences/Flight Sciences Departments, particularly to evaluate the velocity gradient term typical in the aerodynamic heating equations.

$$\approx \left[\frac{J\left(\frac{dV}{dx}\right)_{\text{Flat Faced Cyl.}}}{J\left(\frac{dV}{dx}\right)_{\text{Sphere}}}\right]\left(\frac{V_{vac}}{R}\sqrt{2\rho_1/\rho_s}\right) \qquad (34)$$

where the right hand expression in parentheses is the stagnation point velocity gradient of a spherical surface, thus permitting evaluation of the gradient by using the same radius as for the assumed flat faced cylinder, R = 2.5 in., or half the width of the instrumented plate shown in Fig. (7), when the bracketed ratio value is available as a function of freestream Mach No. from experimental data, Reference (5) as follows:

Mach No.	Ratio $\left[\frac{J(dV/dx)\text{Flat}}{J(dV/dx)\text{Sphere}}\right]$
1	(0.50)
2	.45
3	.42
4	.40
5	.38

(For Mach No. $M_1 = \sqrt{\frac{2}{k-1}\frac{T_s - T_1}{T_1}} = \sqrt{\frac{2}{0.23}\left(\frac{1510}{2900}\right)} = 2.13$,

the corresponding experimental ratio is about 0.45, and with

$$\rho_1/\rho_s = (p_1/p_s)(T_s/T_1) = (2120/13950)\ (4410/2900) = 0.231,$$

the stagnation velocity gradient is evaluated as

$$\left(\frac{dV}{dx}\right)_s = 0.45\ \frac{10,100}{2.5/12}\sqrt{2 \times 0.231} = 14,800\ \text{sec}^{-1},$$

and $\sqrt{14,800} = 121.7$

h_w = wall enthalpy, assumed at 120 BTU/lb, as a representative cold wall condition, and

h_s = total stagnation enthalpy of the plume gas at the upstream condition, already evaluated above as 2040 BTU/lb along with the calculation for V_{vac}

for convenience, giving for the wall loss effect
$(1 - 120/2040) = .941$

Combining the factors evaluated above to show use of consistent units, Eq. (33) now yields

$$q_s = 2.59 \times 1.175 \times 121.7 \times 1.02 \times .941 = \underline{355 \text{ BTU/ft}^2\text{sec}},$$

as the Hoshizaki stagnation heating rate for Data Point No. 2. With the radiation heat transfer added, the total heat transfer rate becomes $355 + 22 + 180 = \underline{557 \text{ BTU/ft}^2 \text{ sec}}$, or about half the experimental 1100 BTU/ft^2 sec.

There is some possibility that the latter test value may be too high since study of the article by Gardon (Reference 6) describing the constantan foil-heavy copper disc heat-sink type of calorimeter used indicates that the reliable limit of application (at least as of the time of the article, 1953) was only 125 cal/cm^2 sec, or 470 BTU/ft^2 sec. This limit was set because of the softening temperature of the thermocouple solder, which may have been exceeded. Hence, the calibration based on assumed linearity of the thermocouple emf-intensity relation may not have held at the high temperatures involved. However, assuming that the test value for Data Point No. 2 may be accepted as valid, a second alternate solution based on a turbulent flat plate heating condition was made.

2. Turbulent Flat Plate Heating

This analysis is based on Reynold's modified skin friction relationship, the Blasius flat surface skin friction formulation, and Eckert's reference enthalpy method (Reference 7). The heating rate is based on the product of a turbulent heat transfer coefficient, H_T, and the available enthalpy difference between the recovery enthalpy, h_{reT}, and the wall enthalpy, h_w:

$$q_T = H_T (h_{reT} - h_w) \qquad (35)$$

where the coefficient is empirically defined from test data as

$$H_T = 0.0358 (g\rho_s V_x)^{0.8} \left(\frac{\mu_s}{x}\right)^{0.2} \qquad (36)$$

The density (lb/ft^3), evaluated at stagnation conditions (p_s = 13950 psfa, T_s = 4410°R, Rg = 67), is:

$$g\rho_s = p_s/R_g T_s \qquad (37)$$

$$= 13950/67 \times 4410$$

$$= 0.0472 \text{ lb/ft}^3$$

The viscosity, μ_s, also evaluated at stagnation temperature, may be approximated by weighting the separate viscosities of the principal exhaust gases (CO_1, CO_2, H_2O), at 0.5, 0.25, 0.25, and 0.07, 0.08, 0.08, respectively, or:

$$\mu_s \approx (f_1 \mu_1 + f_2 \mu_2 + f_3 \mu_3 + \ldots)(\text{ctp})(6.72 \times 10^{-4} \text{ lb/ft sec ctp}) \qquad (38)$$

$$\approx (.50 \times .07 + .25 \times .08 + .25 \times .08)(6.72 \times 10^{-4})$$

$$\approx 5 \times 10^{-5} \text{ lb/ft sec.}$$

Local velocity, V_x, results from the assumption that the flat plate stagnation velocity gradient of 14,800 sec^{-1} remains constant across the transverse flow length x = R = 2.5 in. or 0.208 ft, or:

$$V_x = \left(\frac{dV}{dx}\right)_s x \qquad (39)$$

$$= 14,800 \times 0.208$$

$$= 3080 \text{ ft/sec.}$$

Combining the evaluated factors, the turbulent heat transfer coefficient becomes

$$H_T = 0.0358\ (0.0472 \times 3080)^{0.8} \left(\frac{5 \times 10^{-5}}{0.2083}\right)^{0.2}$$

$$= 0.0358 \times 53.7 \times 0.189 = 0.363 \text{ lb/ft}^2 \text{ sec.}$$

With stagnation enthalpy h_s = 2040 BTU/lb, as before, and local enthalpy

$$h_x = h_s - \frac{V_x^2}{2gJ} \qquad (40)$$

$$= 2040 - \frac{(3080)^2}{50,000}$$

$$= 1850 \text{ BTU/lb},$$

the recovery enthalpy is determined to be:

$$h_{reT} = h_x + 0.18 \left(\frac{V_x}{100}\right)^2 \qquad (41)$$

$$= 1850 + 0.18 \left(\frac{3080}{100}\right)^2$$

$$= 2020 \text{ BTU/lb}$$

Substituting the values found for H_T and h_{reT} in Eq. (35) with 120 again assumed as the cold wall enthalpy, the turbulent flat plate heating rate becomes:

$$q_T = 0.363 \ (2020 - 120)$$

$$= 690 \text{ BTU/ft}^2 \text{ sec.}$$

This result, with the estimated radiation rate from the non-impinging plume, 22, and from the shock disc, 180, together now indicate a predicted total heat transfer rate at Data Point No. 2 of 892 BTU/ft^2 sec. This total is in fair agreement with the test value (81%). Further investigations along these lines to establish realistic relationships between the plume impingement environments and the results of prior experimental studies are desirable over a wider range of cases to provide additional verification of the method.

C. Heat Transfer Rate vs. Impingement Pressure Relation

The turbulent heat transfer method of analysis presented above gives a correlation as good as can be expected in view of the rather sporadic test data available for the sea level plume impingement. The duplicate instrumented data point located at the symmetrically opposite hold-down unit from Data Point No. 2 in the SA-5 launch recorded jagged peaks and valleys about 20% of the averaged maximum value of 1100 BTU/ft^2 sec. However, since even this good agreement may have been fortuitous, considering the numerous assumptions that had to be made in the analysis, a different type of check method would be desirable. Observation of an apparent relationship between experimental heat transfer rates and the well-correlated theoretical and experimental impingement pressures indicate a possible basis for this new method. For example, the two maximum recorded heat transfer rates for

Data Point No. 1 were widely divergent, namely 380 and 780 BTU/ft^2 sec. If the simple linear ratio of the test $q_c/p_I = 1100/97 = 11.4$ BTU/ft^2 sec per psi for Data Point No. 2 is applied directly to the maximum recorded impingement pressure of 46 psia of Data Point No. 1, the resulting 525 BTU/ft^2 sec supports the average of the two values within about 10%.

This q/p_I ratio would not be expected to be linear for other locations in the same plume or for other plumes and impingement environments. It will be shown subsequently that the fraction of the total energy flux of the jet plume transferred to the receiving instrumentation is very small for dense booster plumes ($\sim$.8 of 1%) while it rises considerably, along with the q/p_I ratio for the tenuous high altitude plumes, as would be expected from the decrease in cushioning effect. The few cases available where both the heat transfer rates and impingement pressures were measured simultaneously and accurately are not sufficient to determine this variation at the present time. However, the following analysis presents a basis for exploring the relationship and for planning future experimentation with this concept in mind.

Let the general relationship for the ratio be defined as:

$$q_I = c_q^* p_I \qquad (42)$$

where q_I = total convective heat transfer rate, BTU/ft^2 sec, due to impingement,

p_I = local impingement pressure, lb/ft^2, absolute.

and c_q^* = the ratio of the heat transfer rate to the impingement pressure.

Looking at the dimensions of c_q^* for clues as to its characteristics, we find that one reduced dimension could be BTU/lbsec, a possible specific heat per unit of impulse. Or, preferably expanding BTU x J to ft lbs of work done per ft^2 per sec per lb/ft^2 of impact pressure, the reduced dimensional unit becomes "ft/sec", a pseudo-velocity somewhat analogous to the pseudo-velocity called characteristic velocity ("c*") of a rocket combustion chamber which, however, is related to its capability for producing chamber gas pressure per unit propellant mass flow rate per unit of throat area $p_c/(\dot{w}/gA_t)$, or "specific pressure." Similarly, the concept of c_q^* can be interpreted as the characteristic or specific heat transfer capability with respect to the easily measured or calculated impingement pressure.

The ceiling value for the heat transfer rate per sq ft would be the maximum energy per lb of fluid, or the total enthalpy, h_s BTU/lb, times the corresponding weight flow rate per unit area, w/A. The very small fraction of the total energy flux which cannot be diverted by the flow stream during impingement is here designated as f_1, (a variable, for different plume and

impingement environments). Applying the continuity law, $\dot{w} = g\rho_1 A_1 V_1$, the impingement heat transfer rate may be expressed as:

$$q_I = f_1 \frac{dQ}{Adt} = f_1 \left(\frac{\dot{w}}{A_1}\right) h_s J$$

or
$$q_I = g J f_1 \rho_1 V_1 h_s \tag{43}$$

The total enthalpy of the plume stream is related to the upstream conditions by:

$$h_s = h_1 + V_1^2/2gJ = V_1^2/2gJ\eta_1$$
$$\eta_1 = 1 - T_1/T_s \tag{44}$$

and
$$T_s = T_1 + V_1^2 \left(\frac{2gk}{k-1} R_g\right)$$

where h_1 = static enthalpy due to p_1, ρ_1, T_1

$g = 32.2$ ft/sec^2

$J = 778$ ftlb/BTU

k = gas specific heat ratio, c_p/c_v

R_g = gas constant ftlb/mole lb °R

and T_s = total stagnation temperature, °R.

Now combining the above defined equivalents of q_I and p_I (normal) results in an expression for the heat transfer characteristic velocity:

$$c^*_q = \frac{q_I}{p_I} = \frac{g f_1 \rho_1 V_1 h_s J}{p_1 + \rho_1 V_1^2} \tag{45}$$

Concrete values illustrating the new concepts may be obtained by use of parameters previously evaluated for Data Point No. 2:

$$\rho_1 = 3.4 \times 10^{-4} \text{ slugs/ft}^3$$

$$V_1 = 5900 \text{ ft/sec},$$

$$h_s = 2040 \text{ BTU/lb}$$

$$p_I = p_s = p_1 + \rho_1 V_1^2 = 13950 \text{ psfa}$$

together with the corresponding measured heat transfer rate, $q_c = 1100$ BTU/ft^2 sec, the quantities under discussion are shown in the following tabulation. In addition, this table includes numerical values of the quantities for one test case of the high altitude Apollo S/M RCS engine plume impingement with $q_c = 16$ BTU/ft^2 sec, $\rho_1 = 8.8 \times 10^{-7}$, $V_1 = 9400$ and, coincidentally, $h_s = 2040$.

Parameter	Units	SA-5 Booster Plume*	Apollo S/M RCS Plume**
dQ/Adt	BTU/ft^{2}sec	132,000	54
$\dot{w}/A_1$	lbs/ft^{2}sec	65	0.027
q_I	BTU/ft^{2}sec	1100	16
f_1	-	0.008	0.03
p_I	lbs/ft^2(abs)	13950	78
c_q^*	(BTU/ft^{2}sec)/(psia) "ft/sec"	11.4 61	30 160

*For Data Point No. 2.

**For a parallel side plate distance, $h/R_e = 3$, but normal impingement into a turbulent zone.

Equation (45) apparently would give a zero value for c_q^* with $V_1 = 0$, thus lacks sufficient generality to include the effects of thermal radiation and its associated radiation pressure, and does not isolate the separate contribution that a stagnated gas would make without turbulence. Figure 8(a), (b), and (c) illustrate proposed test setups that would

(a) provide pure radiation without contact of the hot gas with the face of the calorimeter;

(b) provide the heat transfer contribution of a stagnated gas with no transport velocity, and

(c) provide the customary combined heat transfer rate that would be measured by a calorimeter for the case of normal impingement.

Consideration of the separate inputs results in the more precise definition of the characteristic velocity of heat transfer as:

$$c_q^* = \frac{q_r + q_s + q_f}{p_r + p_s + p_f} \qquad (46)$$

where q_r = heat transfer due to impact by impinging photons (radiation)

q_s = heat transfer due to impact by impinging molecules in accordance with the kinetic theory of gas pressure, without apparent transport velocity at the stagnation pressure conditions, but certainly with a statistical root mean square velocity and molecular flow rate which can be calculated. Conduction through a laminar static gas film would best describe this contribution.

q_f = heat transfer due to additional impact by molecules directed toward the surface by steady and unsteady vortex or eddy effects (turbulent heating). The case of heat transfer due to the principal toroidal vortex in equilibrium might possibly be tested and analyzed, together with the stagnation case. However, even if simply the difference between the heat transfer of the two isolated modes (8a) and (8b) and the normally measured total heat transfer (8c) could be evaluated, such a test program would be expected to result in an advance in the state-of-the-art.

Equation (46) now permits an interesting limiting evaluation of the characteristic velocity parameter to be made. For a "non-impinging" plume,

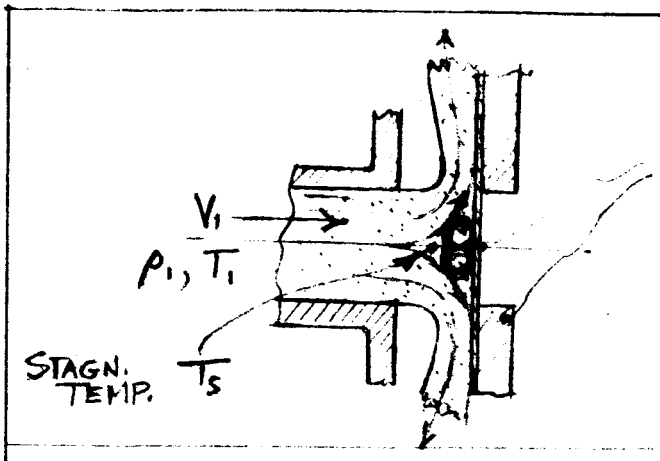

(c) COMBINED HEAT TRANSFER MEASURED BY CALORIMETER

$(q_r + q_s + q_f)$

where q_f includes additional heat transfer due to vortex friction, turbulence, etc.

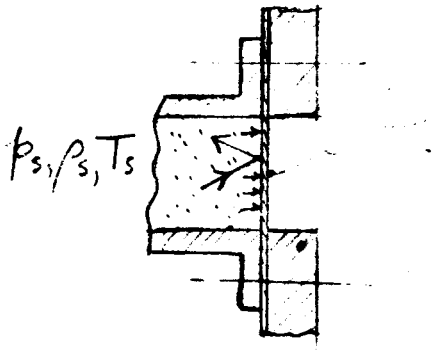

(b) RADIATION PLUS HEAT TRANSFER DUE TO MOLECULAR IMPINGEMENT AT STAGNATION PRESSURE

$(q_r + q_s)$

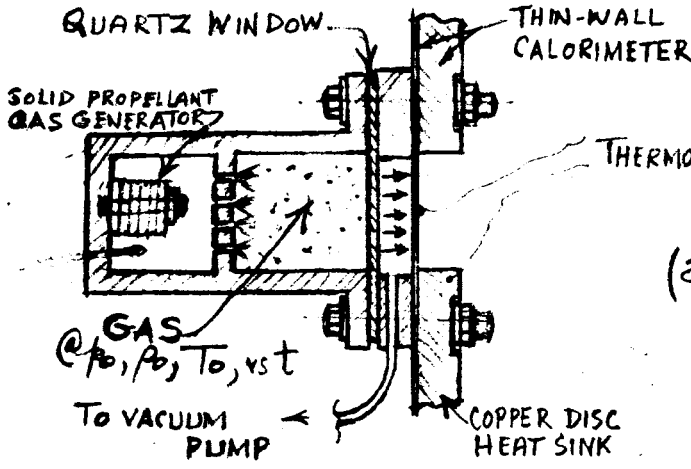

(a) PURE RADIATION, (q_r) DUE TO NET PHOTON IMPINGEMENT AND ABSORPTION

Figure 8: Proposed Test Setups for Isolating Basic Concepts of Heat Transfer due to Rocket Jet Impingement

the incident photons, in reality, do impinge on the surface of the thin-walled calorimeter. The maximum radiation heat transfer from the hot stagnation or shock disc layer to a cold black body receiver would be σT^4, or 180 BTU/ft^2 sec as previously found for Data Point No. 2 of the SA-5 launch data. The radiation pressure due to impingement and capture of these photons is very low, but calculable with a bit of imagination permitting a "non-existent rest mass" to have density:

$$p_r = \frac{F}{A} = \frac{\dot{m}c}{A} = \frac{\rho A c^2}{A} = \rho c^2 \tag{47}$$

$$q_r = \sigma T_s^4 = \frac{\dot{m}c^2}{A} = \frac{\rho A c^3}{A} = \rho c^3 \tag{48}$$

and

$$\text{"}\rho\text{"} = J\sigma T_s^4/c^3 \tag{49}$$

$$= 778 \times 0.475 \times 10^{-12} \times 4410^4/(0.983 \times 10^9)^3$$

$$\approx 1.5 \times 10^{-22} \text{ slug/ft}^3 \text{ (for D.P. No. 2)}$$

The amazing simple and somewhat startling result of dividing Eq. (48) by Eq. (47) directly, without worrying about the nature of "ρ", now gives the absolute ceiling value of the characteristic velocity as:

$c_q^* = \rho c^3/\rho c^2 = c$, the velocity of light!

Fig. (9) shows this limiting value plotted as log-log c_q^* vs log "h_{sc}".

(The same ceiling value would result for the characteristic velocity of the photon rocket engine concept, from $c^* = g p_c A_t/\dot{w} = F/\dot{m} = \dot{m}c/\dot{m} = c$, while the flat plate engine "nozzle" thrust coefficient would be $c/c^* = c/c = 1$. Since the plate pressure is simply a reverse impact (acceleration instead of deceleration) the two ceiling values of the characteristic velocity are evidently not only related, but one and the same for relating the energy flux and pressure in the limiting case.)

A practical result of the foregoing exercise in imaginative analysis is to conclude that the radiation pressure may be dispensed with in the denominator of Equation (46) for the more typical heat transfer cases, while retaining the desired radiation rate in the numerator. It is also convenient to omit the extra pressure p_f due to the unknown vortex or eddy effects, leaving the empirical evaluation of f_1 applied to the whole of the

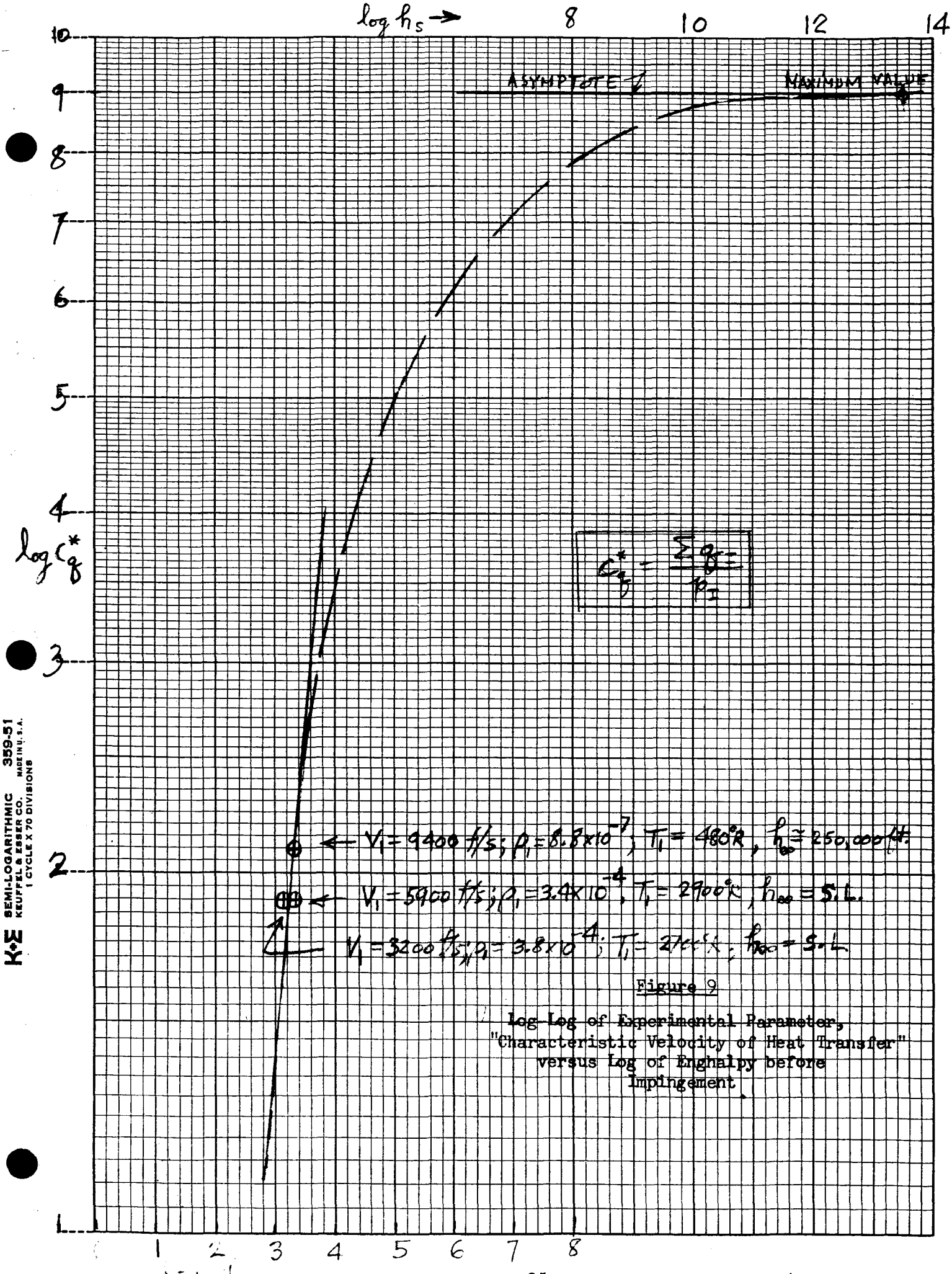

K+E SEMI-LOGARITHMIC 359-51
KEUFFEL & ESSER CO. MADE IN U.S.A.
1 CYCLE X 70 DIVISIONS

Figure 9

Log Log of Experimental Parameter, "Characteristic Velocity of Heat Transfer" versus Log of Enghalpy before Impingement

theoretical numerator, for predicting the total heat transfer relative to the calculable impingement pressure. It is believed that a special test program designed to develop empirical values of the ratio of the heat transfer to impingement pressure could yield some very promising new results and help advance the state-of-the-art.

V. PLUME RADIATION STUDY *

A. Estimated Radiation During Saturn SA-5 Launch

The method for the radiant heat transfer calculations applicable for use in the correlation of the SA-5 sea level launch data was described in detail in the Second Quarterly Progress Report, but since the results were not available at the time of issue, they are here presented.

Results for Data Point No. 2 (Calorimeter 15B 1 & 2)

Time from lift-off, secs	2.0	2.8	3.8
Distance from nozzle exit (x/R_e)	9.2	20.3	35.8
Radial Distances (R/R_e)	-1.1	0	+1.6
Heat Transfer Rates, $BTU/ft^2 sec$			
(a) For single plume	12.7	21.4	9.8
(b) For multiplume (est.)	12.7	21.4	19.6

These results are for the radiation from the non-impinging plume. Additional radiation of about 180 BTU/ft^2 sec from the high temperature region of a normal shock disc was estimated directly from the Stefan-Boltzmann law for use in the correlation with experimental values. As anticipated, the radiation from both the viewed plume and the shock disc are small compared to the convective heat transfer when high impingement pressures occur.

B. Effect of Geometrical Error in Equation for Received Power

In the previous quarterly progress report (Reference 2) it was pointed out that an error had been made in the equation for radiant power received by a surface element. Equation (40) in the First Quarterly Progress Report (Reference 1) should have read

$$P = \iiint \left[\sin \Phi_r \sin \Phi + \cos \Phi_r \cos \Phi \cos (\theta - \theta_r)\right] \left[\int_{\nu_0}^{\infty} I_\nu d\nu\right] \cos \Theta \, d\Phi \, d\theta \quad (50)$$

* The material presented in this section is based on the results of the study made for Power and Environmental Systems by Dr. E. P. French, of the NAA/S&ID Aerospace Sciences/Space Sciences Laboratory.

but the first term in brackets was originally taken to be

$$\left[\cos(\phi - \phi_r) \cos (\theta - \theta_r) \right]$$

which is correct only when either θ_r or $\theta = 0$.

The incorrect form of the power equation was used to compute the results presented in Reference (1).

In order to determine the effect of the error on previous results, one set of cases was recomputed with the correct power equation. The worst case was chosen, namely, an element located one nozzle radius from the axis in the exit plane. Figure (10) compares the previous results (solid lines) and the corrected results (dashed lines). As may be seen, there is no difference when $\theta_r = 0°$ and very little for $\phi_r = 30°$. This indicates that the results for the other cases previously reported are probably in little error since for large distances from the plume (R/R_e = 10 or greater) θ_r will be less than 30° for all strongly radiating regions of the plume.

C. Relationships for Radial Particle Flow

Under heading J: "Particle Concentration Correlation," of the previous quarterly progress report, the second paragraph was incomplete in its description of the particle concentration "N_p", and should have read as follows:

Assume that particles in the plume are confined to a cone centered on the nozzle axis whose apex is at the nozzle throat and whose half angle θ_L is determined by the limiting streamline for a particular size. Assume further that the particle concentration N_p is a function of the distance X from the apex and that the particle velocity V_p is constant in magnitude and directed along streamlines from the apex, as shown in the following sketch,

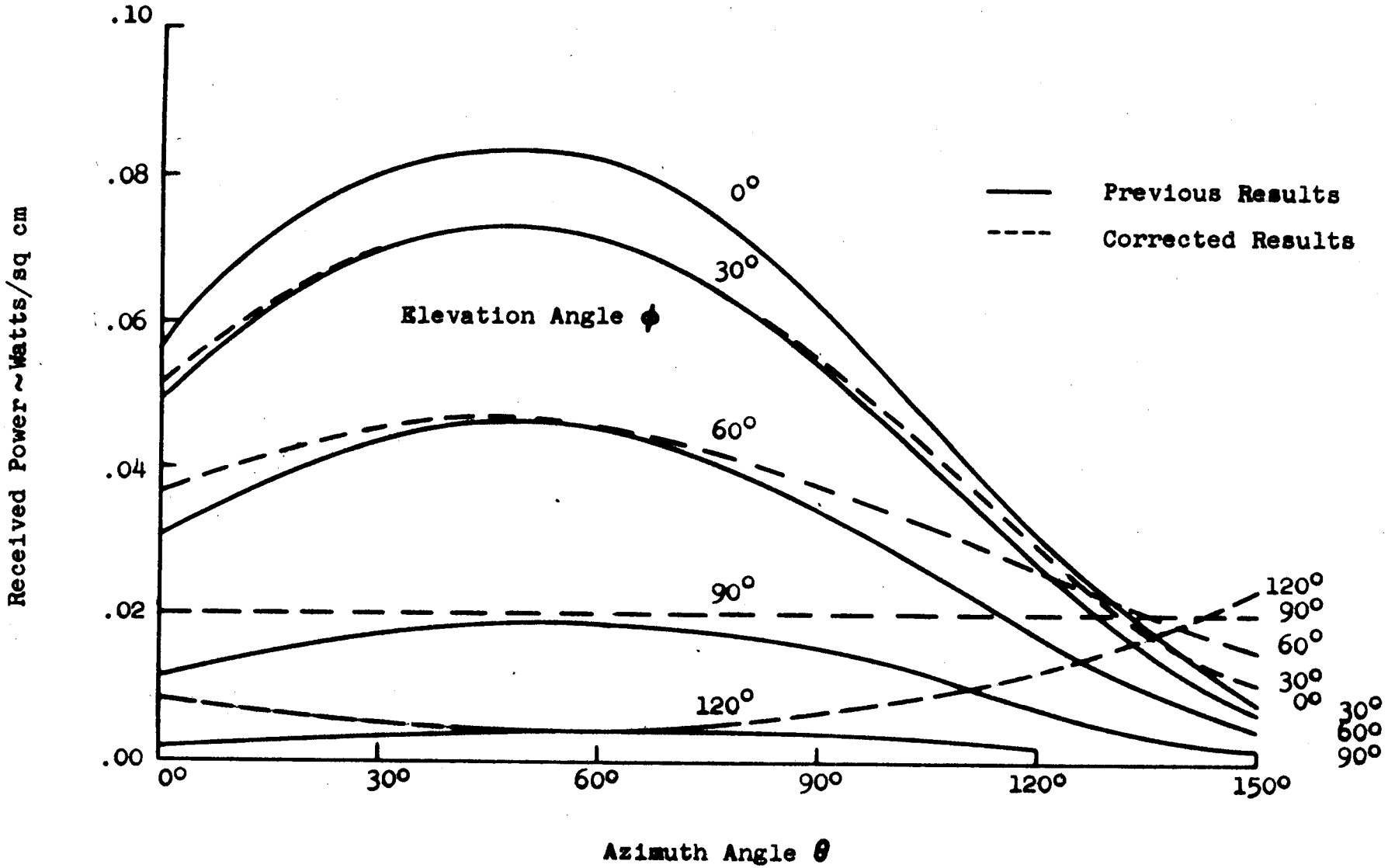

Fig.10. Comparison of Corrected Results for Received Power (Eq. 50) with Previous Results

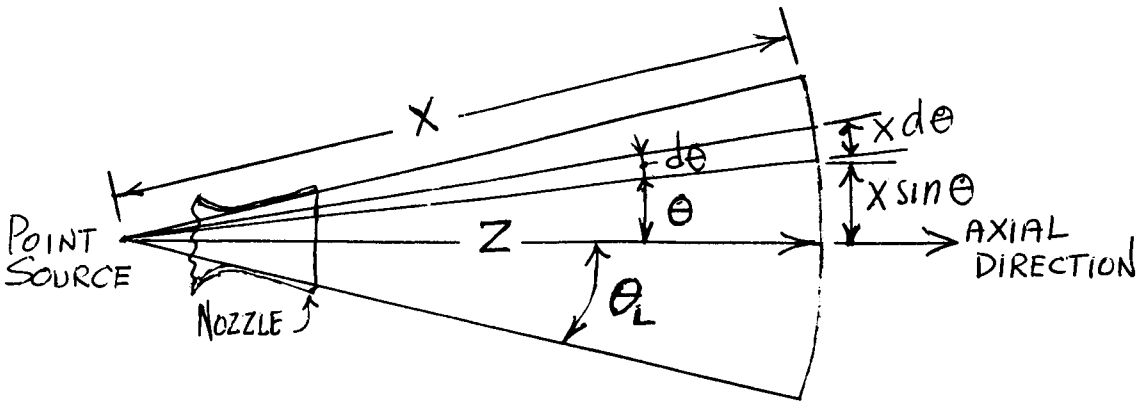

Under these circumstances the particle mass flow $\dot{M}_p$ through any surface X = constant becomes

$$\dot{M}_p = 4/3\ \pi r_p^3\ \rho_p\ N_p\ V_p\ A(X) \qquad (51)$$

(previously Eq. 18, p. 39 of Reference 2)

The area A(X) enclosed by the limiting streamlines $\pm\ \theta_L$ is found by integrating an annular element $dA = 2\pi(X \sin\theta)(Xd\theta)$ from 0, to $\theta = \theta_L$, or in terms of the axial distance Z from the apex since $X = Z/\cos\theta$:

$$A(X) = 2\pi Z^2 \frac{\sin\theta d\theta}{\cos^2\theta}$$

$$= 2\pi Z^2 \left[1/\cos\theta\right]_0^{\theta_L}$$

$$= 2\pi Z^2 \left[(1/\cos\theta_L) - 1\right]$$

Expanding $\cos\theta = 1 - \theta_L^2/2 + \ldots.$

$$A(X) \approx 2\pi Z^2\ (\theta_L^2/2) \approx \pi Z^2\ \theta_L^2 \qquad (52)$$

giving the particle mass flow $\dot{M}_p$ in terms of axial distance Z, as

$$\dot{M}_p = 4/3\pi^2\ r_p^3\ \rho_p\ N_p\ V_p\ Z^2\ \theta_L^2$$

and the particle concentration, as given in the previous Eq. 19, with $V_p = kVg$:

$$N_p = \frac{\dot{M}_p}{4/3\ \pi^2 \rho_p V_g} \left[\frac{1}{r_p^3\ kZ^2\ \theta_L^2} \right] \qquad (53)$$

where the term in brackets depends on the particle size and nozzle geometry.

VI. DISCUSSION OF RESULTS AND RECOMMENDATIONS FOR FUTURE WORK

This third quarterly progress report completes the presentation of the results obtained within the Phase I Analytical and Phase II Correlation portions of the program. During the next quarter period, the material presented in Quarterly Progress Reports Nos. 1, 2, and 3 will be reviewed and coordinated into the comprehensive single Final Report due at the close of the contract period.

The additional results included in the present report on the effects of changes in the variables entering into the calculation of the jet plume boundary when the freestream interaction is considered serve to support a concept of plume influence coefficients as a useful tool in plume determination. This approach toward handling the great number of possible combinations of jet plume parameters and environmental conditions is recommended for inclusion in a continued program of investigation. Since the deviations in the plume contraction ratio versus freestream Mach number are shown to be relatively small for at least two of the input parameters (k and θ_N), it is considered feasible to derive plume descriptions over a wide range of conditions from a small set of selected "standard" reference plumes at sea level and low altitudes, at some intermediate altitude, or altitudes, and at high or near-vacuum altitudes.

The derivations of the equations for the sine of the true angle of impingement of streamlines on a variety of curved surfaces is presented with enough detail to permit clear understanding of the analysis technique used. Continued work to expand the results into a general equation suitable for computer programming is recommended.Since experimental data for rocket plume impingement on curved surfaces are not available, additional special tests designed to prove out the equations for the curved cylindrical and spherical surfaces are recommended.

One of the two alternate aerodynamic heating methods presented in this report, the turbulent flat plate heating analysis, was successful in raising the total predicted level of the heat transfer rate to about 80% of the maximum measured rate for the Saturn SA-5 launch data analyzed. The investigation of the variety of aerodynamic heating solutions which were originally based on satellite reentry studies and data, indicates that continued effort should be spent on improving them specifically for the case of rocket jet impingement heating effects. Correlation studies should be continued, as additional reliable experimental results become available. In addition, basic studies and test programs are recommended, along the lines of the proposed isolation of the radiative, conductive, and convective modes of heat transfer in the test

setups discussed. The new approach to the solution of heating problems suggested by the concept of the "characteristic velocity" of heat transfer may yield valuable insight into the true mechanism of energy transfer involved.

The additional material in the section on plume radiation shows that the earlier version of the equation for incident received power is only slightly in error. The simpler equation thus may be completely adequate for prediction in most cases, with the exact solution reserved for special cases.

REFERENCES

1. SID 64-1896: Quarterly Progress Report No. 1 on NASA/MSFC Contract NAS 8-11407: Engineering Method to Predict Saturn V Vehicle and Launch Complex Environments due to Rocket Jet Impingement, 15 October 1964, North American Aviation, Inc., Space and Information Systems Division, Downey, California

2. SID 65-44: Quarterly Progress Report No. 2 on above Contract, 15 January 1965

3. Kindle, J. H. Theory and Problems of Plane and Solid Analytic Geometry, Schaum's Outline Series, Schaum Publishing Company, New York, 1950

4. Cose, D. A. and Lee, B. T.: Heat Transfer from an Impinging Jet, Technical Note, p. 173, AIAA Journal, V. 3 n 1, January 1965

5. Boison, J. C., and H. A. Curtiss: An Experimental Investigation of Blunt Body Stagnation Point Velocity Gradient, J.A.R.S., V. 29, No. 2, February 1959

6. Gardon, R.: An Instrument for the Direct Measurement of Intense Thermal Radiation, Review of Scientific Instruments Vol. 24, n 5., May 1953

7. Eckert, E.R.G.: Survey on Heat Transfer at High Speeds, WADC Technical Report 54-70, U.S. Air Force, April 1954.